Flow Characterization and Current Technical Research Issues of The Hiest Hypersonic Facility

Hideyuki TANNO and Katsuhiro ITOH
Japan Aerospace Exploration Agency, Kakuda Space Center
1-Koganesawa, Kimigaya, Kakuda Miyagi 981-1525
JAPAN

tanno.hideyuki@jaxa.jp and ito.katsuhiro@jaxa.jp

ABSTRACT

The test flow characteristics of the free-piston driven high-enthalpy shock tunnel JAXA-HIEST are described. Based on the tuned operation theory, the facility can exclusively produce world-record level high stagnation enthalpy (up to 25 MJ/kg) and high stagnation pressure (up to 150 MPa) for 2 ms or longer. With conical or contoured nozzles, re-entry test models up to 500 mm in length at a 50-degree angle of attack can be available under free-stream test flow at 7 km/s with the unit Reynolds number 5 million per meter. These characteristics are attributed to a remarkable thermally harsh free-stream condition, and given the short test duration on the order of ms, aerodynamic or aeroheating measurements in HIEST entail several technical issues. The current status of research on these issues is also discussed.

Nomenclature

H	=	enthalpy, MJ/kg
P	=	pressure, Pa
$\dot{q}$	=	heat flux, MW/m^2
Re	=	Reynolds number
St	=	$\dot{q}/\rho u H$, Stanton number
T	=	temperature, K
U or u	=	velocity, m/s
ρ	=	density, kg/m^3
C_D	=	Drag coefficient
C_L	=	Lift coefficient
C_M	=	Pitching moment coefficient

Subscripts

0	=	Stagnation condition
∞	=	Free-stream condition

1.0 INTRODUCTION

In the latter half of the 1980's, Japan began research on a winged re-entry vehicle to be launched by the H-II rocket, named HOPE (H-II Orbiting Plane) [1]. In parallel, researches on a hypersonic air-breathing engine also began for a prospective SSTO spaceplane. To ensure progress in the research on aerothermodynamics and propulsion for these space transportation system programs, the need for hypervelocity ground testing became apparent. In an attempt to solve these technical requirements, the National Aerospace Laboratory of Japan (NAL), the predecessor of JAXA, had an enterprising and ambitious plan to build a large free-piston shock tunnel to obtain aerothermodynamic data from the ground testing. To build a knowledge base for the design of the large free-piston shock tunnel, several experimental studies on the characteristics of free-piston

shock tunnels mainly for the free-piston driver were conducted using small- and medium-sized pilot facilities [2][3], and supported by numerical simulations [4]. The most remarkable result from these preliminary studies was the establishment of the tuned-operation method [5,6] that improves the performance of a free-piston driver, while simultaneously ensuring safe operation.

In 1998, a large facility named the High Enthalpy Shock Tunnel (HIEST) was finally built to achieve tuned operation meeting the requirements for testing the aerothermodynamic characteristics of HOPE and those for the scramjet engine tests [7]. The velocity range in the flight path to be tested was 3 to 7 km/sec, corresponding to stagnation enthalpy of approximately 4 to 25 MJ/kg. A conical nozzle was designed for test models up to 500 mm in length. Considering the time required for flow establishment and force measurements with test models up to 500 mm in length, the test flow duration should be longer than 2 ms at the maximum enthalpy condition. The conical nozzle was designed for aerothermodynamic tests mainly for HOPE-scaled models. The flight Mach number was 8 to 25 with dynamic pressure up to 100 kPa. A contoured nozzle was also designed for scramjet engine combustion tests. The flight Mach number for the scramjets ranged from 8 to 14 with dynamic pressure up to 500 kPa.

This report first describes the design principle, operation and basic performance of HIEST, followed by a discussion of the technical issues facing the facility, nozzle throat melting, flow establishment within the HIEST test duration, and the effects of impurities in the free-stream.

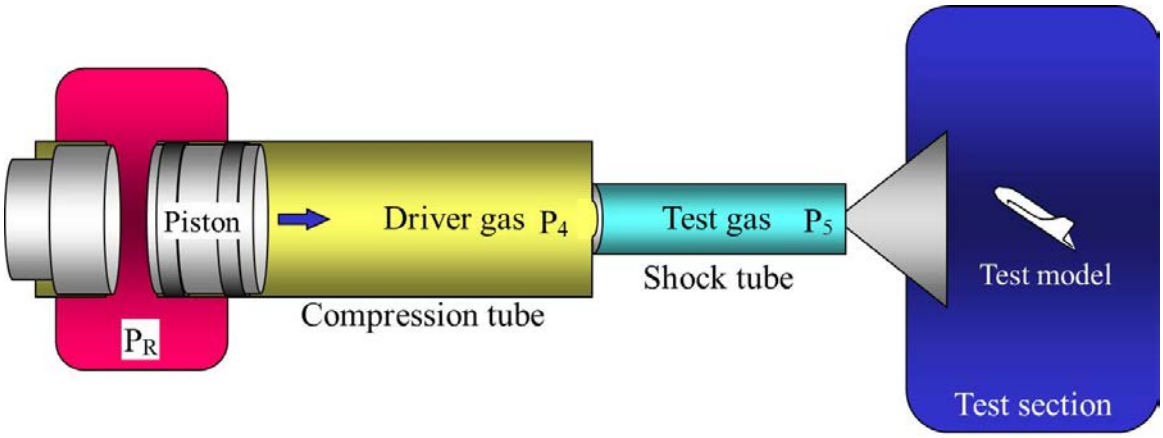

Figure 2-1: Schematic illustration of the free-piston shock tunnel

2.0 FACILITY CONFIGURATION

As illustrated in Fig. 2-1, a free-piston shock tunnel consists of a secondary reservoir (high-pressure air reservoir), compression tube, shock tube, nozzle, and test section. The compression tube and shock tube are partitioned with a diaphragm, and filled with driver gas and test gas, respectively. Helium or a mixture of helium and argon is typically used as the driver gas, and dry air or pure nitrogen gas is typically used as the test gas. Fig. 2-2 depicts the operation procedure of the facility. Opening the quick valve at the secondary reservoir launches a piston into the compression tube that travels down the tube. The piston compresses the driver gas until the diaphragm ruptures. A high-speed shock wave is initiated in the shock tube by the drainage of compressed driver gas into the shock tube. High-temperature and high-pressure test gas is produced at the end of the shock tube through the shock wave reflection process. The stagnation enthalpy and pressure depend on the compression ratio and composition of the driver gas, diaphragm rupture pressure, and initial pressure of the driven gas. Very high stagnation enthalpy of up to 30 MJ/kg can be achieved with a compression ratio of up to 70. As the volume of driver gas becomes small, however, constant driver gas pressure cannot be maintained, resulting in a significant decline in shock tube performance. The tuned

operation method was developed to improve free-piston driver performance by operating the piston at a sufficiently high speed to maintain constant driver gas pressure, and then decelerating it by using the driver gas remaining after the test period until the piston stops upon arriving at the end of the compression tube.

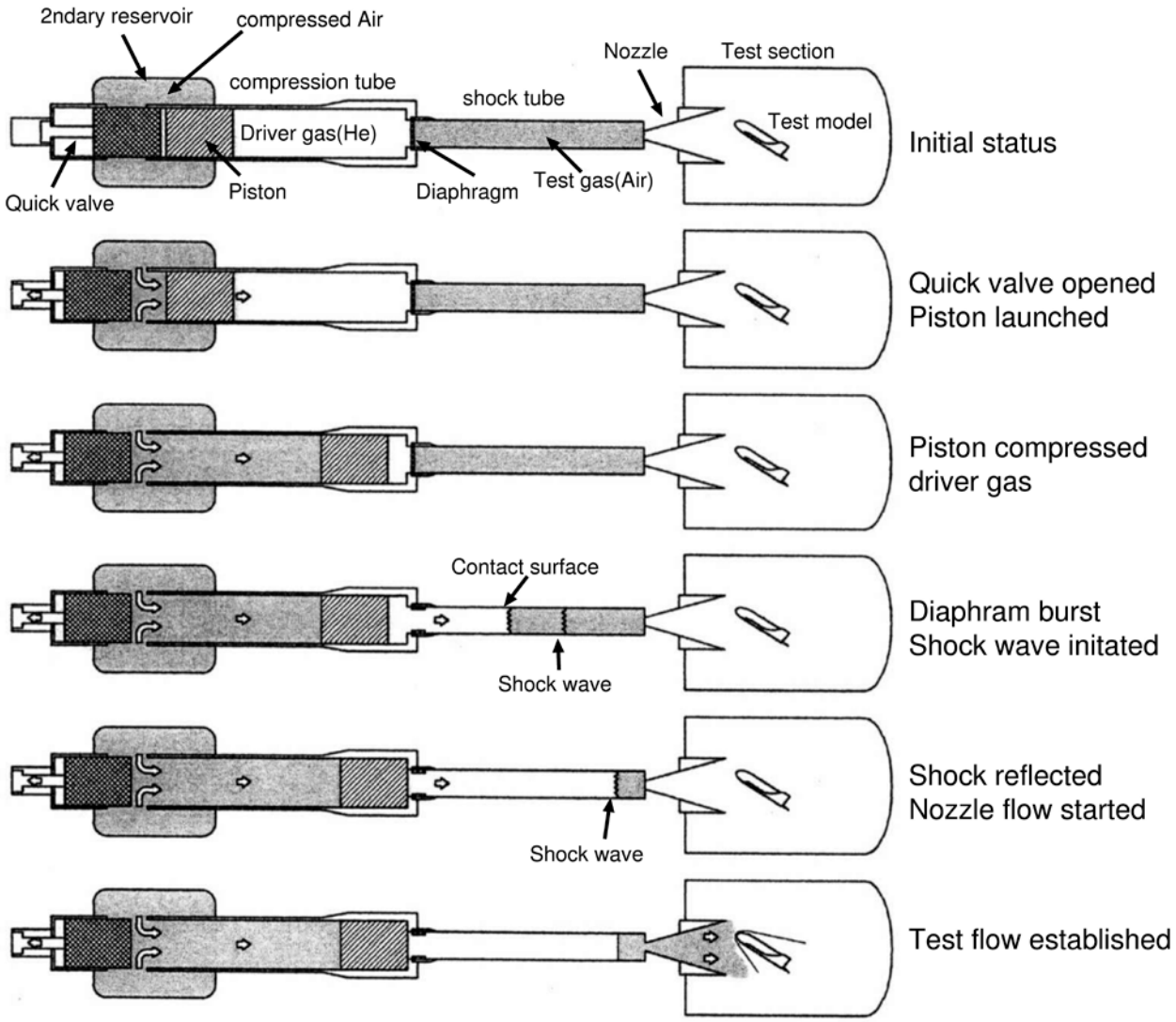

Figure 2-2: Operation procedure of the free-piston driven shock tunnel

As the free-piston shock tunnel HIEST was designed to satisfy the requirements of HOPE aerothermodynamic tests, stagnation temperature and free-stream density were the principal factors in reproducing chemical non-equilibrium effects. The velocity in the flight path flow to be tested ranged from 3 to 7 km/sec, corresponding to a stagnation enthalpy range of about 4 to 25 MJ/kg. The maximum test model size was 500 mm in length. Considering the time needed for flow establishment and force measurement with a test model of 500 mm in length, the test flow duration should be longer than 2 ms at the maximum enthalpy condition.

For the scramjet engine tests, the flight Mach number to be tested ranged from 8 to 14 and the corresponding stagnation enthalpy range was involved in the lower part of the HOPE test range, but required higher dynamic pressure of 100 kPa or more. The expected model engine size to be tested was 2 m; therefore, a longer test flow duration in a lower enthalpy condition and a larger test section were required. To satisfy

these different testing requirements, the nozzle reservoir condition and geometries were determined first. In order to reduce the time spent for a nozzle starting in a higher enthalpy condition and enlarge the exit diameter for the test at a large angle of attack, a conical nozzle measuring 2.8 m in length with an exit diameter of 1200 mm and 12 degrees in half angle pressure was designed for the HOPE tests. Conversely, scramjet engine testing requires higher dynamic pressure and parallel flow, as opposed to the size of the core flow. Therefore, a contoured nozzle measuring 2.8 m in length with an exit diameter of 800 mm and a smaller area ratio was also designed.

After the nozzle designs, a decision was made to have the shock tube diameter and length satisfy the test time requirements, in considering the effect of the boundary layer growing in the shock tube behind the incident shock wave on reducing the test gas slug-length, as well as the early arrival of driver gas. Finally, a decision was made to determine the diameter and length of the compression tube, and the piston mass based on the tuned operation theory. Table 2-1 lists the specifications of HIEST. Fig. 2-3 shows overall views of the facility.

Table 2-1: HIEST specifications

Compression tube	42 m in length	600 mm in diameter
Shock tube	17 m in length	180 mm in diameter
Piston mass	220, 290, 440, 580, 780 kg	
Nozzle (conical)	1.2 m in exit diameter	24 - 50 mm in throat diameter
Nozzle (contoured)	0.8 m in exit diameter	50 mm in throat diameter
Maximum stagnation enthalpy	25 MJ/kg	
Maximum stagnation pressure	150 MPa	
Test time	2 msec or more	

Figure 2-3: Photographic views of HIEST. (Left) Overview from the secondary reservoir; (Right) Conical nozzle, test section and dump tank.

3.0 FACILITY CHARACTERISTICS

3.1 Tuned operation

As described in the previous section, the free-piston shock tunnel produces a driver gas at high pressure and high temperature through adiabatic compression by a free piston. In a conventional free-piston shock tunnel, the piston speed should be kept low so as not to cause serious damage to the facility. In large-scale facilities that use very heavy pistons, however, this could create serious damage. When using a low-speed piston, the

compression tube pressure drops rapidly after the main diaphragm ruptures due to the small volume of driver gas remaining after the free-piston compression process. The shock Mach number regarding travel down the shock tube was thus decreased due to this drop in driver gas pressure. As a solution to this drawback, the over-driving operation concept originally proposed by Stalker has already been applied to several free-piston shock tunnels to improve their performance. In the theory, the compression tube pressure will be maintained with high residual piston speed after the diaphragm bursts. However, to avoid a significantly higher risk of high-speed piston collision at the end of the compression tube, it is again necessary to reduce piston speed to achieve a soft landing at the end of the compression tube.

The operating condition that simultaneously overcomes the overdriving and soft landing is called a tuned operating condition. The tuned operating condition in FPST was first carried out by Stalker, who assumed a constant driver gas condition following diaphragm rupture. Meanwhile, the study of Stalker was based on the assumption of constant piston deceleration. For large-scale facilities with a massive piston under high-speed operation, these assumptions were not valid to predict safe operating conditions. Therefore, the accuracy of predicting piston motion must be improved. Itoh conducted an analytical study of piston motion at an infinite compression ratio, and later expanded his research to devise a formula that can predict piston motion at a finite compression ratio. He also proposed a new concept for soft landing operation that utilizes a piston buffer at the point where the piston motion trajectory in the x-t diagram has a saddle point. His theory was demonstrated in small- and medium-scale free-piston shock tunnels, followed by the development of the enormous facility JAXA-HIEST.

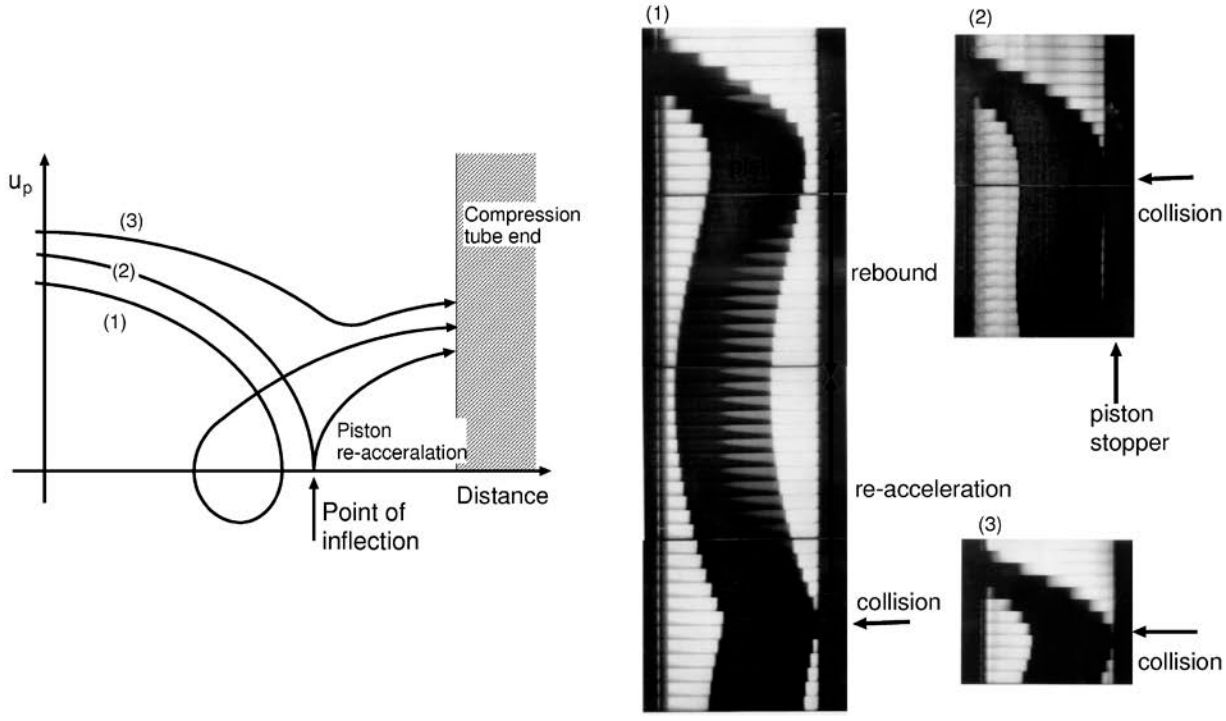

Figure 3-1: Piston speed-up at the end of the compression tube. (1) Rebound mode, (2) Soft landing mode, and (3) Direct mode.

3.1 Piston final motion

After the rupture of the diaphragm, the piston motion in FPST can be categorized into three regimes. Fig. 3-1 shows (1) Rebound mode, (2) Soft landing mode, and (3) Direct mode. It is obvious that the direct impact of the piston at high speed on the compression tube wall has a disastrous effect. Even in rebound mode, where

the piston's kinetic speed at diaphragm rupture is minimum, the piston retains its momentum when striking the end of the tube, due to piston re-acceleration after the rebound. If the tube is operated with a relatively low volumetric compression ratio, the collision speed is still high enough to cause serious damage. In the case of soft landing mode, the piston speed is zero at the inflection point. If the piston is trapped near this point, the piston collision speed is minimum theoretically. Under the present soft landing operation concept, the appropriate length of a piston buffer is used to catch the piston there.

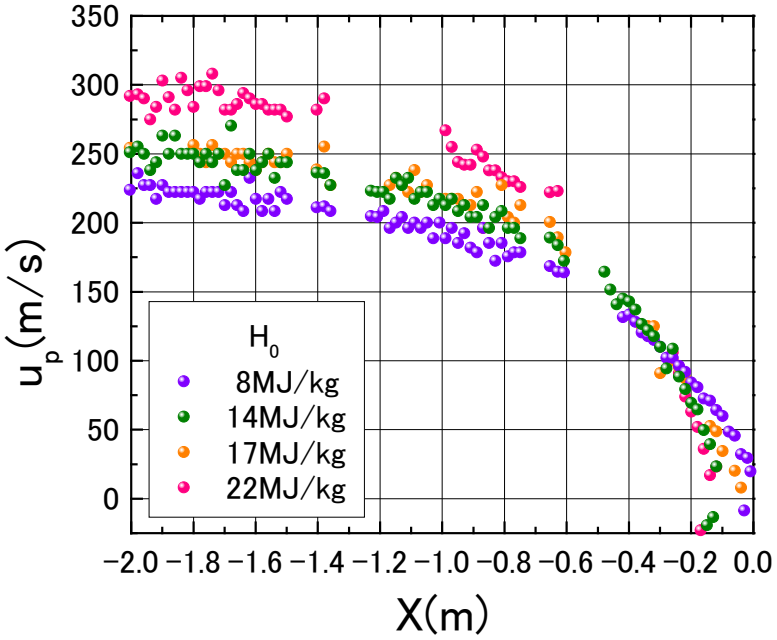

Figure 3-2: Measured piston speed-up at the end of the HIEST compression tube

3.2 HIEST general performance

As mentioned above, the tuned operation method effectively enables the safe holding of driver gas pressure, resulting in improved shock tube performance. The tuned operation can be achieved by tuning the piston mass and pressure to push the piston to the driver gas condition, so as to ensure the right piston speed at diaphragm rupture, with the piston and driver gas having matched momentum and energy. In order to check piston control, the piston motion was measured using a simple laser reflection method in HIEST. The pressure was also measured at the end of the compression tube to evaluate the effect of the tuned operation. Fig. 3-2 shows the piston speed versus distance from the end of the compression tube in stagnation enthalpy of 8, 14, 17 and 22 MJ/kg, as estimated from the piston detector signal. The diaphragm ruptures when the piston arrives at 900 to 700 mm from the end. The precise position of the piston at diaphragm rupture depends on the operating conditions. The results show that the piston has the right speed of around 200 m/sec necessary for holding driver gas pressure, and arrived at the end when its speed became almost 0.

Fig. 3-3 shows the driver gas pressure traces recorded at the end of the compression tube (top) and the shock tube (bottom) at H_0 = 13 MJ/kg and P_0 = 83 MPa. The timing of diaphragm rupture is indicated in the top figure and the pressure could be held for several milliseconds as expected, demonstrating the effect of the tuned operation. As a result, the nozzle reservoir pressure behind the reflected shock could be held as well, and good pressure recovery was obtained, as shown in the bottom figure. The recovery of pressure also depends on the length-to-diameter ratio of the shock tube L/D, as well as the holding time of the driver gas pressure. A larger L/D indeed gives a longer test time but attenuates the shock wave more. As

the increase in test time is limited by viscous effects, there is an appropriate L/D to compensate for the increase in test time and the suppression of shock wave attenuation. For the HIEST design, parametric CFD was conducted to find the appropriate value, and L/D was determined to be 95. The general characteristics of the nozzle flow are reviewed with the pitot pressure profiles shown in the next section. In case of the contoured nozzle, the size of the core flow area is more than 600 mm and large enough for aerodynamic testing with a 500-mm test model.

As mentioned in the introduction, HIEST was originally built for the design of the Japanese winged re-entry vehicle HOPE, and the tunnel's performance matches a binary scaling parameter with test models that are 4% (500 mm in length) of the actual flight vehicle size (a full-scale total length of 20 m). The top chart in Fig. 3-4 shows the operation envelope of HIEST in the relation between stagnation enthalpy and binary scaling for the re-entry flight path of HOPE. With stagnation pressure up to 150 MPa, HIEST can be also produce high Reynolds number test flows on the order of 1 x 10^6/m. The bottom chart in Fig. 3-4 shows the relation between the stagnation pressure and unit Reynolds number in HIEST. At the maximum stagnation pressure, note that HIEST can produce a unit Reynolds number of 3 x 10^6/m even at stagnation enthalpy of H_0 = 20 MJ/kg. As the transition Reynolds number at hypersonic flow is taken to be around 4x10^6, HIEST is thus suitable for boundary layer transition studies under high enthalpy conditions.

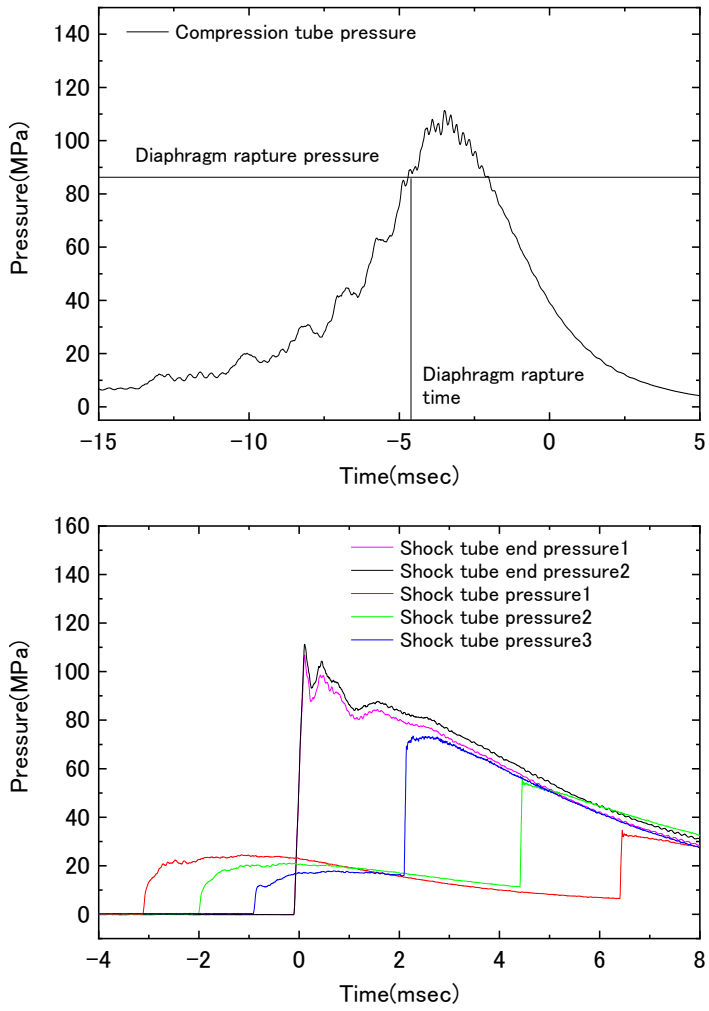

Figure 3-3: Compression tube (top) and shock tube pressure (bottom) records at the tube end

under H_0 = 13 MJ/kg and P_0 = 83 MPa

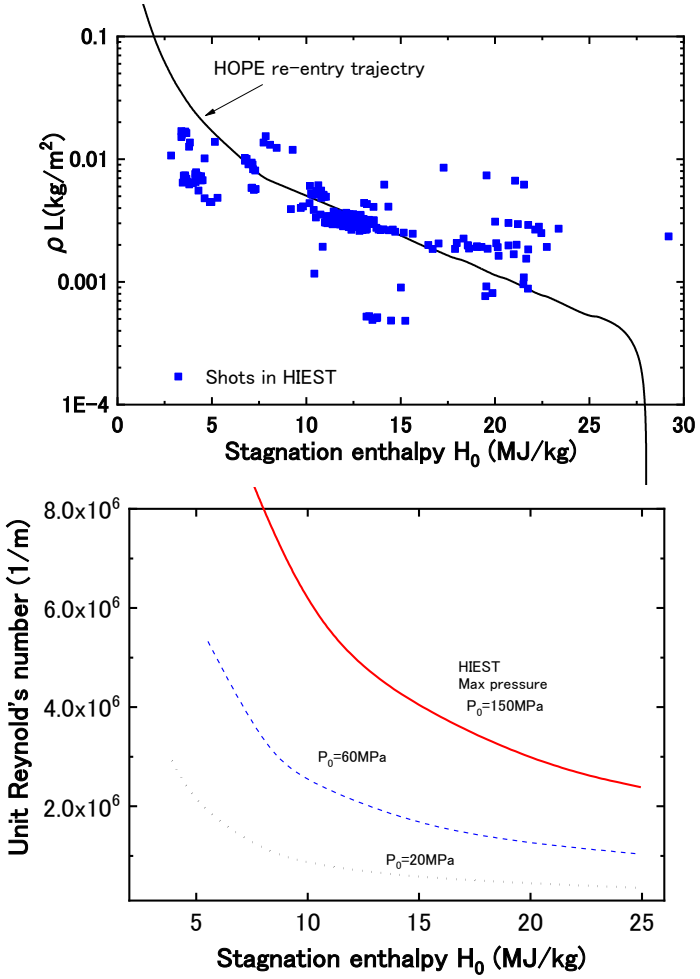

Figure 3-4: HIEST operation envelope. Binary scaling parameter and stagnation enthalpy (top). Small squares show the condition tested in HIEST. Reynolds number and stagnation enthalpy (bottom).

4.0 TECHNICAL ISSUES

4.1 Nozzle throat melting

Due to a higher stagnation condition (temperature and pressure) and longer test time, the thermal load occurring at the HIEST nozzle throat is much more severe than that in other existing facilities. This harsh environment causes nozzle throat melting or even evaporation, which significantly degrades test flow quality. Fig. 4-1 shows an example of the pitot pressure traces (top) and surface heat flux traces (bottom) in the HIEST test free-stream with a CZC (Cr-Zr-Cu) copper alloy throat. In both pressure and heat flux traces, the onset of large fluctuations were observed after a certain time following test flow establishment. Given the increase in stagnation enthalpy, the fluctuations began earlier and became more serious. This fluctuation trend suggests that the nozzle throat melting or evaporation is associated with this fluctuation phenomena.

The CZC melting point is 1357K and indeed a mark of melting was clearly observed after a high-enthalpy shot (Fig. 4-2 left).

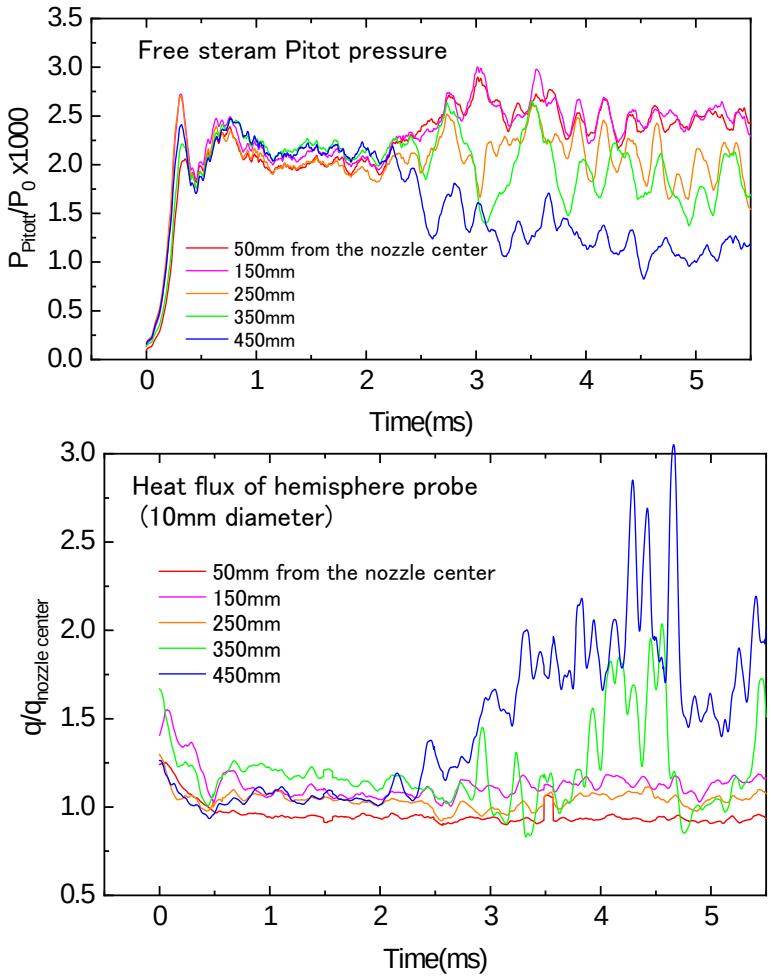

Figure 4-1: Free-stream pitot pressure (top) and hemisphere heat flux records (bottom) at the HIEST conical nozzle exit with the CZC throat (H_0 = 13 MJ/kg and P_0 = 50 MPa). Pressure and heat flux were normalized by values measured at the center of the nozzle.

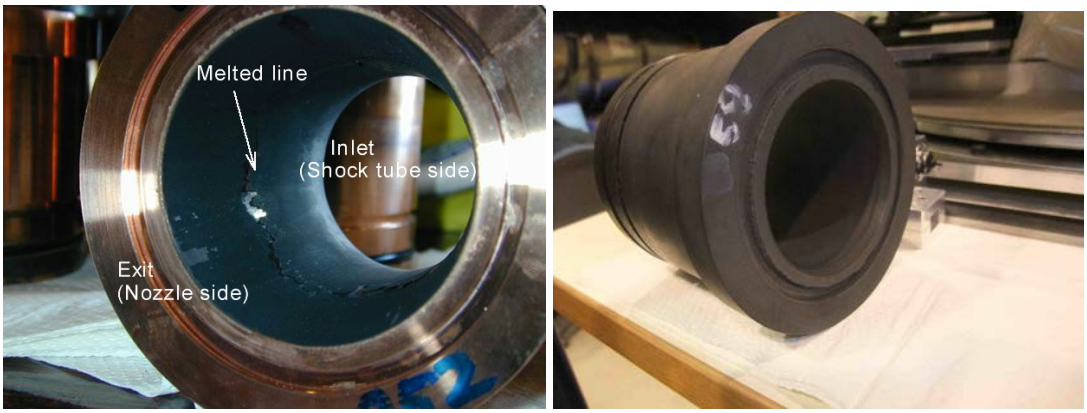

Figure 4-2: Nozzle throat blocks. (Left) CZC high-temperature material; (Right) Graphite nozzle throat. Both pictures were taken after a shot under H_0 = 13 MJ/kg and P_0 = 50 MPa.

To make matters worse, the boundary layer ingestion of heavy metal evaporating from the nozzle throat surface increases the boundary layer thickness, causing the nozzle core flow to shrink. The molybdenum nozzle throat (with a melting temperature of 2860K) was quite effective in mitigating this effect[8]. However, the significantly high cost of the molybdenum throat was unacceptable in obtaining a sufficient number of shots. In order to solve these technical and financial restrictions, a graphite nozzle throat was newly developed (Fig. 4-2 right). Given the smaller momentum of products originating from the graphite nozzle surface than that from the CZC nozzle surface, the effect of boundary layer ingestion is not so severe. Fig. 4-3 shows that the test core was remarkably extended with the graphite nozzle throat. Fig. 4-4 shows the mitigation of heat flux fluctuations.

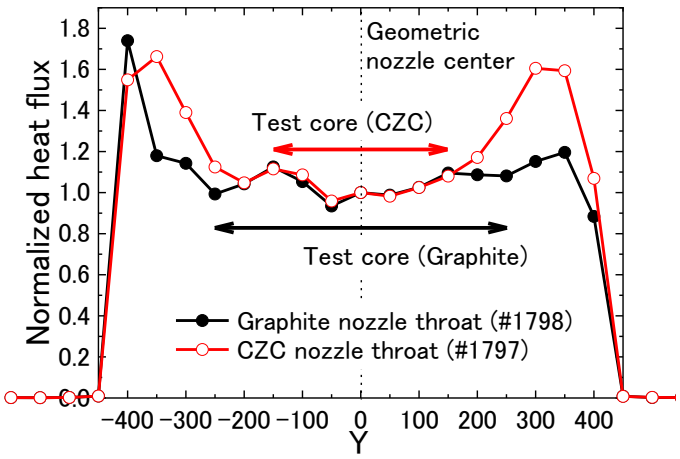

Figure 4-3: Heat flux profiles of the CZC nozzle throat and graphite nozzle throat at the exit of the HIEST contoured nozzle (H_0 = 13 MJ/kg and P_0 = 50 MPa)

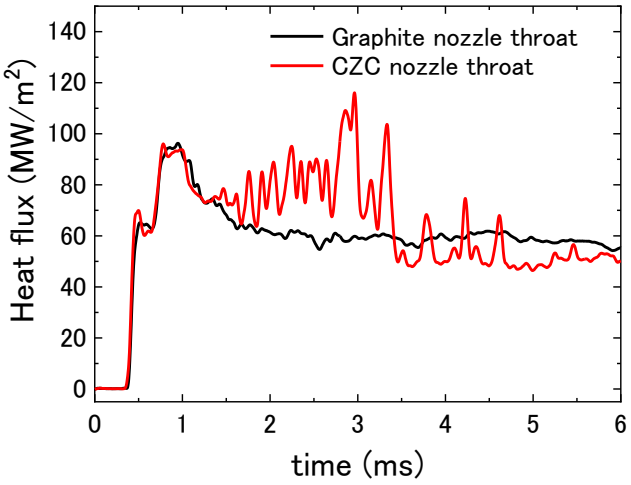

Figure 4-4: Heat flux traces of the CZC nozzle throat and graphite nozzle throat measured with a hemisphere probe (10 mm in diameter) located 300 mm from the center of the contoured nozzle

(H_0 = 13 MJ/kg and P_0 = 50 MPa)

4.3 Flow establishment within short test duration

Flow establishment around the test model is a critical issue for measurements made in impulsive facilities. As the re-entry vehicle models often have a large angle of attack, there should be a large separation area behind the model, for which a longer steady state time is expected to be requested. In aerodynamic tests of the Japanese re-entry vehicle HYFLEX [9] at a 40-degree angle of attack, the three-component aerodynamic characteristics under high-temperature, real-gas conditions were measured [10]. The pressure of the nose (stagnation pitot pressure) and back surface of the model (Fig.4-5 left) were recorded to observe flow establishment around the model. Fig. 4-5 (right) shows the ratio of pressure at the back surface and at the nose. The ratio clearly shows that there is plateau time, which means the flow becomes almost steady during the short test duration. Moreover, the measured histories of drag, lift, and pitching moment that support the flow around the model became established. Fig. 4-6 shows that the force of all three components showed a steady value as well. The Lift-Drag ratio (Fig. 4-7) agreed quite well with the results obtained in a conventional blowdown wind tunnel (ONERA S4M [11]), which also implied that there was no significant effect due to the short test time.

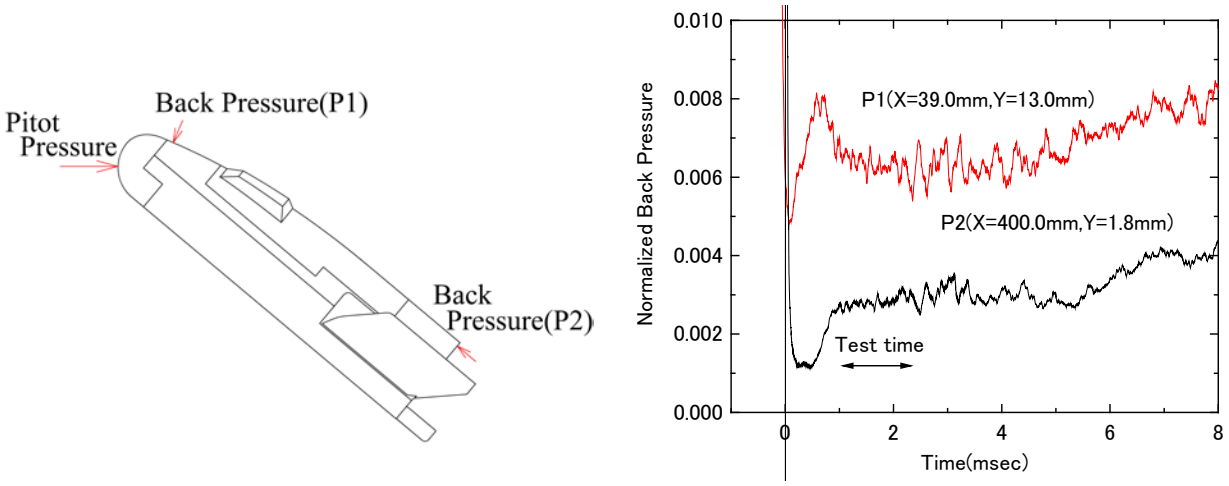

Figure 4-5: (Left) Schematic of the HYFLEX model. Arrows show positions of the pressure transducers. (Right) Pressure traces normalized by free-stream stagnation pressure (H_0 = 13 MJ/kg and P_0 = 40 MPa)

HIEST was originally designed to test scramjet models measuring 2 meters in length, and flow establishment in such a long duct flow was a critical issue for thrust measurements for a test duration on the order of ms. Fig. 4-8 shows a generic scramjet prototype tested in HIEST, which had a very simple duct configuration with a total length of 2.8 meters and a rectangular inlet area of 250 mm (H) x 200 mm (W). The axial force of the scramjet can be measured using the semi free-flight force measurement technique. In even such a long configuration, the internal flow in the scramjet seems steady during short test time monitoring of the drag force histories normalized by the free-stream pitot pressure (Fig. 4-9). It was concluded that the HIEST test time is sufficient for testing a scramjet measuring up to 2.8 meters in length.

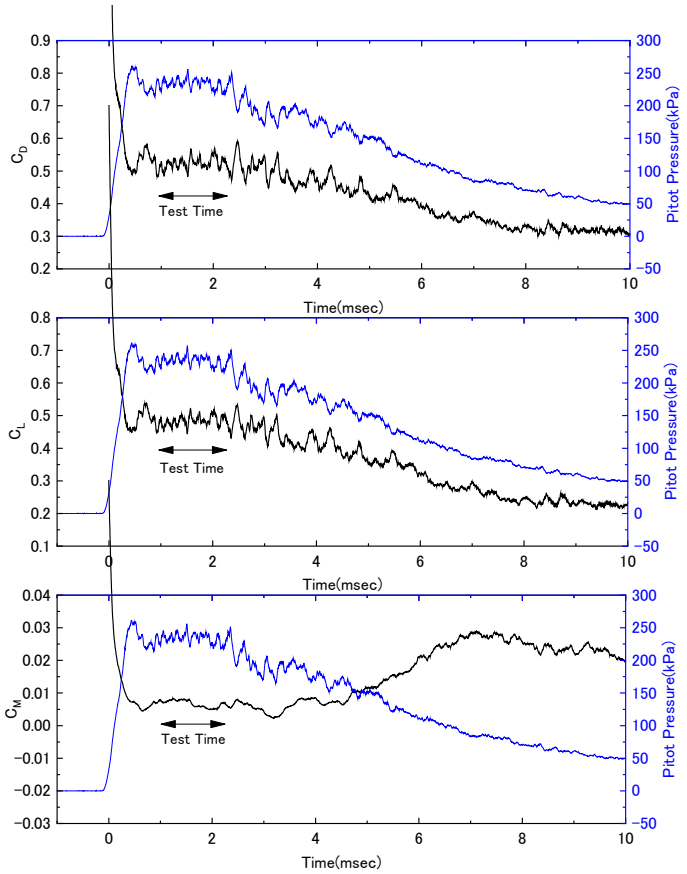

Figure 4-6: Time records of aerodynamic coefficients of the HYFLEX lifting body test model (H_0 = 13 MJ/kg and P_0 = 40 MPa). Drag force coefficient C_D (top), Lift force coefficient C_L (middle), and pitching moment coefficient C_M (bottom) are shown as solid lines. The free-stream pitot pressure history is also shown on each plot as a thin line.

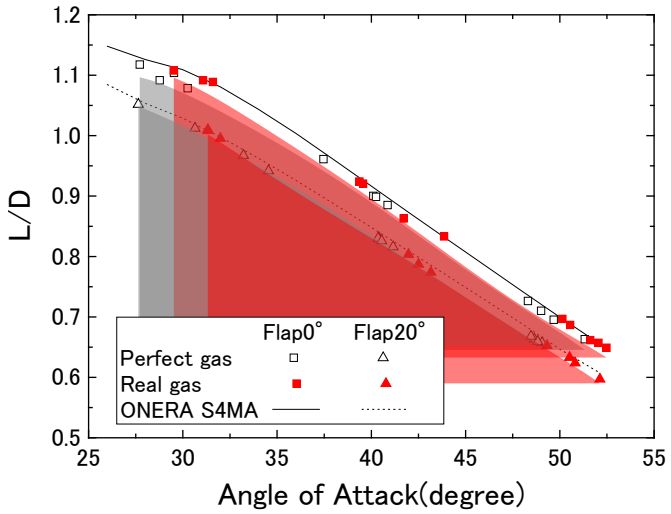

Figure 4-7: Lift-drag ratio of the HYFLEX test model at a 30 to 50-degree angle of attack. Results measured in the conventional blowdown wind tunnel ONERA S4MA are superimposed.

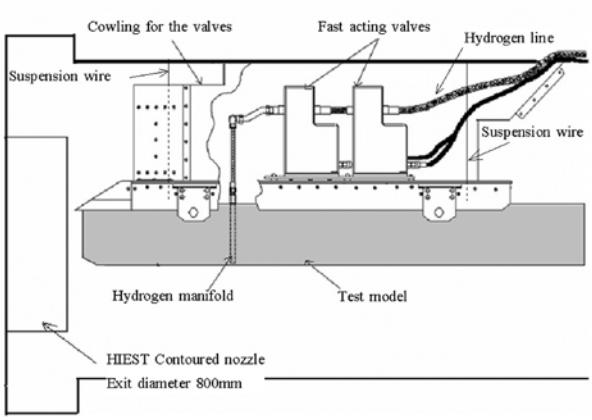

Figure 4-8: A duct scramjet installed in the HIEST test section

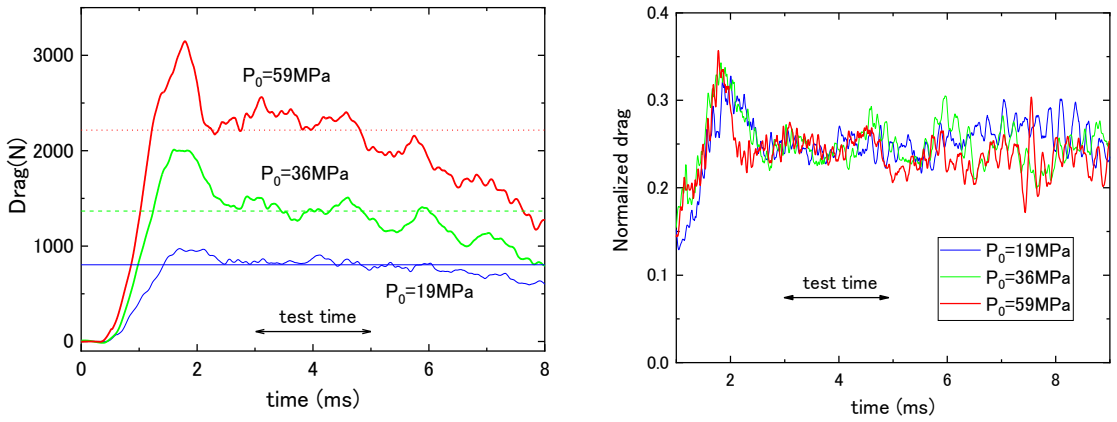

Figure 4-9: (Left) Drag histories of the duct scramjet. Stagnation pressure was varied from P_0 = 19 MPa to 59 MPa. (Right) Drag histories normalized by products of dynamic pressure (half the pitot pressure) and the duct cross-section.

4.4 Impurities in the free-stream

As described in the previous section, free-piston shock tunnels are the only ground test facilities capable of producing reliable aeroheating data in high-stagnation enthalpy and high-pressure flow (i.e. high Reynolds number hot hyperflow). Despite the increasing importance of this type of shock tunnel, there is still the fatal deficiency to disturb accurate aeroheating measurements in the shock tunnels. Hollis [12] summarized the heat-flux results measured in several major shock tunnel facilities to identify the heat-flux uncertainty, and found that some measurements were 20 to 100% higher than numerically predicted. This augmentation was only observed under conditions of high enthalpy and pressure with relatively large-scale models, thereby generating fatal uncertainty in high-enthalpy/high-Reynolds number tests (i.e. those for turbulent aeroheating). In HIEST, this heat flux augmentation was also observed in the 250 mm-diameter Apollo capsule aeroheating test campaign [13]. Fig. 4-10 shows a comparison of measured heat-fluxes (raw data) with the numerical calculation results [14] under H_0 = 13 MJ/kg and P_0 = 83 MPa. From this figure, it is possible to see that the experimentally measured values differ significantly from the numerically calculated values due to the large heat-flux augmentation. At the present condition, measured heat-fluxes were approximately double those of the calculations. Since this augmentation is far more

serious in HIEST, it is essential to investigate this phenomenon in detail and determine its cause.

From previous HIEST aeroheating test campaigns, it was suspected that the augmentation was mainly caused by radiative heating from the bow-shock layer in front of the test models. However, this hypothesis is not convincing because the radiation heating (up to 10,000K) from the air is not significant enough to produce remarkable heating on the order of MW/m^2. To demonstrate the radiation heating hypothesis, a wind tunnel test campaign was conducted [15] using a simple 10-inch diameter circular flat-face model (Fig. 4-11 left) with miniature coaxial thermocouples installed on the front surface. As shown in the schematic of the model surface (Fig. 4-11 right), the special feature of the model is the transparent glass windows (made of UV-grade fused silica - SiO_2) placed in front of some of the installed thermocouples. These glass windows function as optical filters and cut off convective heating, thereby allowing the thermocouples to only sense radiative heating, whereas the thermocouples without windows receive conductive heating, in addition to radiative heating. Fig. 4-12 shows the results measured with the flat-face model at H_0 = 13 MJ/kg and P_0 = 83 MPa. It should be noted that large radiative heat-flux (over 11MW/m^2) measured through the optical window was almost 46% of the heat-flux measured without a window. Table 4-1 shows the averaged heat-flux ratio of radiation heating to total heating estimated for the present Apollo capsule test . In the results, the measurement precision (2σ) was low due to fluctuations of the measured heat-flux histories.

The spectroscopic test campaign was subsequently conducted in HIEST to identify the radiation source. From the visible to near infrared range, the test gas was found to contain sufficient impurities (mainly iron atoms) so as to alter the shock layer radiation, suggesting that the source of radiation is within the shock layer itself [16]. Given the large uncertainty remaining in radiation heat-flux measurements as shown in Table 4-1, an accurate assessment of the radiation heat flux has yet to be made.

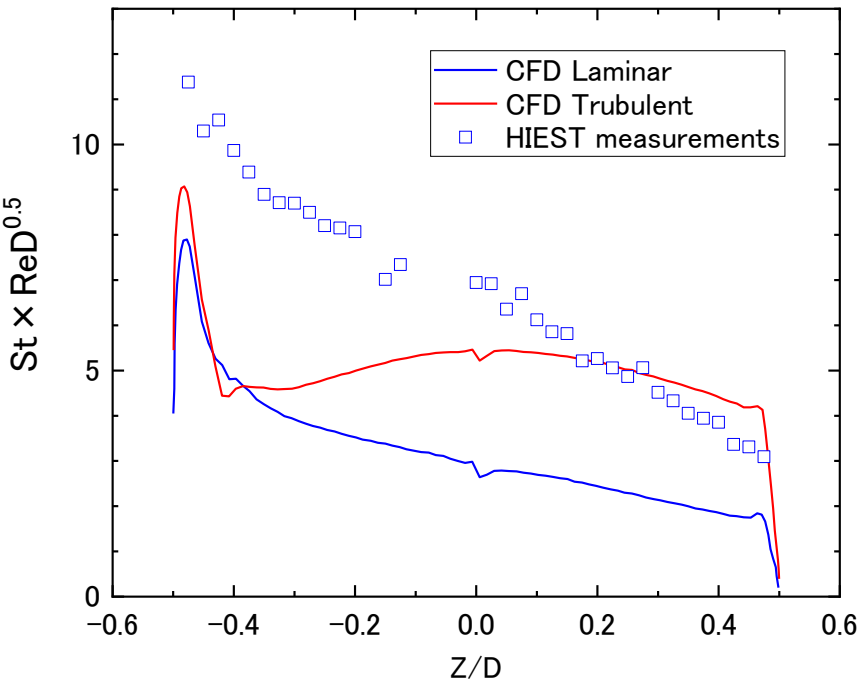

Figure 4-10: Measured heat-flux profiles on the heat shield side of the Apollo capsule model under stagnation enthalpy of H_0 = 13 MJ/kg and stagnation pressure of P_0 = 83 MPa. Numerical results (fully laminar and fully turbulent boundary layer) are also overlapped.

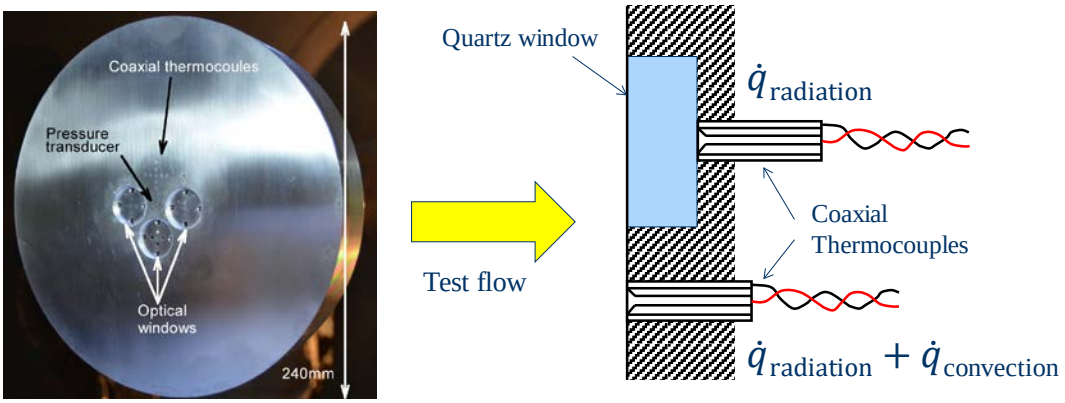

Figure 4-11: (Left) Flat plate test model for radiative heating measurement; (Right) Image of surface thermocouples (flush-mounted and mounted with a quartz window).

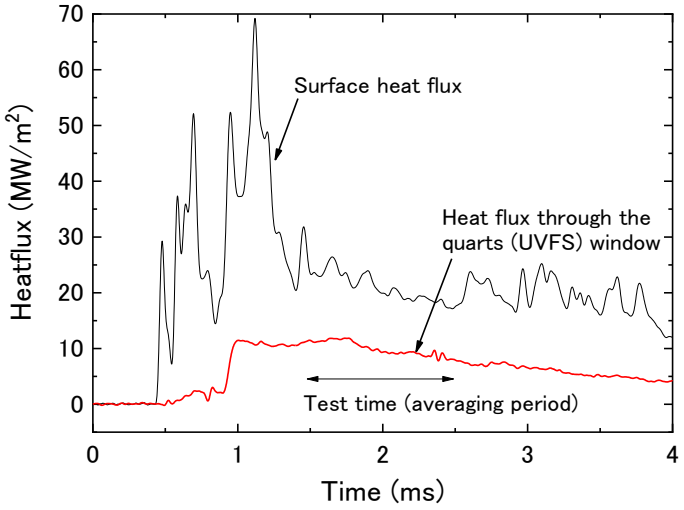

Figure 4-12: Surface and radiative heat-flux on the flat-face model at H_0 = 13 MJ/kg and P_0 = 83 MPa

Table 4-1: Heat-flux measured with the flat plate model

Heat-flux $\dot{q}_0$ (MW/m^2)	Heat-flux through quartz window $\dot{q}_{r0}$(MW/m^2)	Ratio $\dot{q}_{r0}/\dot{q}_0$	Uncertainty 2σof $\dot{q}_{r0}/\dot{q}_0$
24.2	11.1	0.46	±0.12

ACKNOWLEDGEMENT

We wish to express our deepest appreciation for the work done by Mr. Narita and Mr. Fujimura in our laboratory, especially for operating the facility and making data reductions for the study.

REFERENCES

[1] S. Asada, S. Miyake, J. Kouchiyama, T. Akimoto and M. Shirouzu, "Lessons learned from HOPE system designing," AIAA Paper No. 2001-1881, 2001.

[2] H. Tanno, K. Itoh, T. Komuro and K. Sato, "Experimental study on the tuned operation of a free-piston driver," *Shock Waves*, **10**:1-7, 2000.

[3] K. Itoh, S. Ueda, T. Komuro, K. Sato, M. Takahashi, H. Miyajima, H. Tanno and H. Muramoto, "Improvement of Free Piston Driver for High Enthalpy Shock Tunnel," *Shock Waves*, **8**:215-233, 1998.

[4] K. Tani, K. Itoh, M. Takahashi, H. Tanno, T. Komuro and H. Miyajima, "Numerical study of the free-piston shock tunnel performance," *Shock Waves*, **3**:313-319, 1994.

[5] R. J. Stalker, "A study of the free-piston shock tunnel," *AIAA J.*, Vol. **5**, No. 12, pp. 2160-2165, 1967.

[6] H. G. Hornung, "Performance data of the New Free-Piston Shock Tunnel at GALCIT," AIAA Paper No. 1992-3943,1992.

[7] K. Itoh, T. Komuro, K. Sato, H. Tanno and S. Ueda, "Hypersonic aerodynamic research of HOPE using high enthalpy shock tunnel," AIAA Paper No. 2001-1824, 2001.

[8] K. Itoh, M. Takahashi, T. Komuro, K. Sato, H. Tanno and S. Ueda, "Effect of throat melting on nozzle flow characteristic in high enthalpy shock tunnel," Proc. 22nd International Symposium on Shock Waves, pp. 459-464 , 1999.

[9] M. Shirouzu and M. Yamamoto, "Overview of the HYFLEX project," AIAA Paper No. 1996-4524, 1996.

[10] H. Tanno, T. Komuro, K. Sato and K. Itoh, "Experimental study on hypersonic pitch-up anomaly in shock tunnel," Proc. 31st International Symposium on Shock Waves, 2017.

[11] S. Watanabe, S. Ishimoto and Y. Yamamoto, "Aerodynamic characteristics evaluation of hypersonic flight experiment (HYFLEX) vehicle based on flight data," AIAA Paper No. 1996-4527, 1996.

[12] B. R. Hollis and D. K. Prabhu, "Assessment of Laminar, Convective Aeroheating Prediction Uncertainties for Mars Entry Vehicles," AIAA Paper No. 2011-3144.

[13] H. Tanno, T. Komuro, K. Sato, K. Itoh, J. Olejniczak and R. P. Lillard, "Aeroheating measurement of Apollo-shaped capsule with boundary layer trip in the free-piston shock tunnel HIEST," AIAA Paper No. 2014-043, 2014.

[14] L. Kirk, R. P. Lillard, J. Olejniczak and H. Tanno, "Boundary Layer Transition and Trip Effectiveness on an Apollo Capsule in the JAXA High Enthalpy Shock Tunnel (HIEST) Facility," AIAA Paper No. 2015-0209, 2015.

[15] H. Tanno, T. Komuro, R. P. Lillard and J. Olejniczak, "Experimental Study of High-Enthalpy Heat-flux Augmentation in Shock Tunnels," *Journal of Thermophysics and Heat Transfer*, **29**(4):858-862,

2015.

[16] B. A. Cruden, A. M. Brandis, J. H. Grinstead, J. Olejniczak, L. Kirk, R. P. Lillard, H. Tanno and T. Komuro, “Measurement of Ultraviolet Radiative Heating Augmentation in HIEST Reflected Shock Tunnel,” AIAA Paper No. 2015-2512, 2015.